

# A Novel Wideband and Multi-band Implantable Antenna Design for Biomedical Telemetry

Mohamed Behih<sup>1</sup>, Farid Bouttout<sup>1</sup>, Tarek Fortaki<sup>2</sup>, and Christophe Dumond<sup>3</sup>

<sup>1</sup>Department of Electronics, University of Bordj Bou Arreridj, El-Anasser 34030, Algeria  
mohamed.behih@univ-bba.dz, f.bouttout@univ-bba.dz

<sup>2</sup>Departement of Electronics, Batna 2 University, Batna 5000, Algeria  
t.fortaki@univ-batna2.dz

<sup>3</sup>PRISME Institut, IUT of Chartres, University of Orleans, Orleans 45100, France  
christophe.dumond@univ-orleans.fr

**Abstract** – In this work, a novel multi-tracks wide-band and multi-band miniaturized antenna design for implanted medical devices biomedical telemetry is proposed. This antenna entirely covers seven frequency bands which are the bands (401–406) MHz of the Medical Device Radiocommunications Service (MedRadio), the three bands (433.1–434.8), (868.0–868.6), and (902.8–928.0) MHz of the Industrial, Scientific, and Medical (ISM), and the three bands (608–614) MHz, and (1.395–1.400) and (1.427–1.432) GHz of the Wireless Medical Telemetry Service (WMTS). The antenna possesses a compact full size of  $(19.5 \times 12.9 \times 0.456)$  mm<sup>3</sup>. The antenna miniaturization and impedance bandwidth enhancement are achieved using two techniques: the patch slotting and insertion of open-end slots in the ground plane, respectively. Prototype of proposed antenna with multi-tracks has been fabricated and tested in free space. The comparison between the simulated and measured reflection coefficient has been done and found in good agreement with each other. Furthermore, simulations of the proposed antenna implanted in the underneath the scalp in a realistic human model shows a wideband operation from 0.19 to 0.94 GHz, and from 1.38 to 1.54 GHz corresponding to return loss ( $S_{11} \leq -10$  dB). Link budget calculation is performed to specify the range of telemetry considering both Specific Absorption Rate (SAR) restrictions and effective isotropic radiated power (EIRP) limitations. The designed implantable antenna with full ground plane presents an appropriate reflection coefficient for muscle implantation. Furthermore, the designed implanted muscle antenna may be also suitable for skin implantation.

**Index Terms** – Biomedical telemetry, implanted antenna, ISM, MedRadio, multi-band, multi-tracks, wideband, WIMD, WMTS.

## I. INTRODUCTION

Wireless body area network (WBAN), standardized by IEEE 802.15.6 [1, 2] is a promising wireless personal area network to connect low power devices placed on, inside, or around the human body for medical and non-medical ends. Implanted medical devices (IMDs) [2, 3] focus on various clinical purposes: diagnostic, monitoring, therapeutic, etc. [4]. The most modern of IMDs includes a communication mechanism for data exchange [4, 5]. In regard to the traditional limited near-field inductive coupling link [6], an implantable radiofrequency antenna has been integrated into the IMD to establish an effectiveness bidirectional wireless link between them and an exterior monitoring/control base-station for communication and/or physiological data transmission [5–7]. The biomedical telemetry using wireless IMDs (WIMDs) antenna has become more attractive for real-time remote monitoring and allowing telemedicine to improve the patient's life quality [2]. Nowadays, WIMDs are integrated in WBAN, where an on-body (or off-body) sensor node is used for linking the device to the exterior monitoring/control base-station that stands away from the body [4, 8, 9].

The implanted antennas in the heterogeneous lossy medium of the human body are designed for operation in specified frequency bands that face the challenge of size miniaturization while keeping good antenna radiation performances, i.e., high efficiency, high gain, and larger bandwidths [5] to establish an efficient telemetry communication. In addition, the specific absorption rate (SAR) restrictions for patient safety and the antenna biocompatibility also must be considered.

Large available bandwidth is an important factor to keep the implantable antenna performances stable and away from any frequency detuning due to the

dielectric properties modification caused by gender, age, health situation, etc. In addition to this, when such antennas cover several allocated frequency bands, they will allow to increase the WIMDs communication applications diversity. Furthermore, allocated telemetry frequency bands vary from a country to another. In spite of this, low frequencies are associated with relatively lower loss through the biological tissues [3], and the frequency bands in the range (0.2–2) GHz are more efficient for both data transmission and wireless powering [10]. Thus, implantable antennas small enough to fit into WIMDs that cover the almost allocated bands widely within this frequency interval are more attractive. Such antennas are not widely reported in the literature.

Various implantable antennas have been proposed in the literature to cover various frequency bands of WIMDs biotelemetry applications [3, 5]. The developed antennas can be classified in three groups: (1) single narrow band [11] and single wideband [12–21], (2) dual narrow bands [22–25], dual lower wideband [26–28], dual higher wideband [29], and dual wideband [30–31], and (3) multi-narrow bands [32–34], multi-lower wideband [35–37], and multi-wideband [38].

Several miniaturization techniques of implantable patch antennas are reported in [39] such as slots insertion in the radiating patch, stacking [15, 22], and embedded open-end slots in the ground plane [26, 32, 34, 38]. The split ring resonator (SRR) technique is also used [11, 30, 40]. In spite of this, various methods have been proposed to enhance the gain, including the partial meandering of the patch [18], metamaterial array on the superstrate [17], lens and parasitic ring, and reactive impedance surface [19]. The ground plane slotting [26], stacking [21], and a capacitor at the open-end of the ground slot [38] are also used for the impedance bandwidth widening.

In [12] and [15], two muscle broadband implantable PIFA antennas have been proposed for covering the Medical Device Radiocommunications Service (MedRadio) band (401–406) MHz, where the exhibited volumes of 399 and 448 mm<sup>3</sup> are relatively large. Similar study for the 2.45 GHz industrial, scientific, and medical (ISM) frequency band has been carried out in [20], where the occupied volume is 295.75 mm<sup>3</sup> and the impedance bandwidth is 220 MHz.

In [38], a quad-band implantable PIFA antenna for the underneath the scalp in the head muscle and other clinical applications has been proposed where the whole size of the antenna is 8.43 mm<sup>3</sup>. Tests carried out on minced pork and the covered bands are MICS 403 MHz and ISM 915 MHz, both designed for telemetry, whereas the ISM 2.4 GHz is used for control signaling

and the Midfield 1470 MHz is used for wireless power transfer.

In [22] and [24], two scalp dual bands implantable antennas have been proposed. For the first antenna, four frequency bands have been covered. Nevertheless, the simulated bandwidths inside a head model were relatively narrow. The second antenna has been proposed only for intracranial pressure monitoring. Furthermore, the exhibited SAR values were large.

In [32], a scalp triple band implantable PIFA antenna has been proposed. Although the volume is relatively small, the obtained impedance bandwidths were relatively narrow and the SAR has high values at considered frequencies. In [34], another triple band implantable antenna for deep tissue and skin implantations has been designed. The obtained measured impedance bandwidths were narrow and lower biotelemetry frequency bands are not covered.

Recently, in the reference [40], the authors proposed a flexible wideband loop antenna for wireless capsule endoscopy that covers all biotelemetry frequency bands within the range (305–3500) MHz.

In this work, a novel multi-tracks wideband implanted antenna design is proposed for muscle WIMDs telemetry for frequencies up to 2 GHz. Since this allows miniaturization, high permittivity substrates are often used in the design of implantable antennas. However, this also has the effect of reducing the impedance bandwidth. For this reason, the choice was made to achieve miniaturization by an efficient design and to use a low permittivity substrate. Antenna's miniaturization is realized using path current lengthening principle and the optimized size of the design is 114.70 mm<sup>3</sup>. The design procedure starts from an initial coax-feed PCB plate and consists of four steps, in which conducting regions of the patch and the ground plane are shaped by slotting.

The designed antenna performs multi-band operation and covers seven biomedical telemetry frequency bands with large bandwidths available and has the particularity of not having a superstrate.

The paper is organized as follows. In Section II, the antenna structure and the design and optimization process are presented. The fabricated prototype of the implantable antenna is also presented as well as a comparison of measured and simulated return loss in free space.

In Section III, tissues and implantation depth effects are investigated using two phantom models; a one-layer model which consists of skin or fat, and a three-layer model constituted of skin, fat, and muscle. Section IV presents antenna operation in two realistic implantations of human body; in the underneath the scalp and in the

muscle of the upper arm. Far-field gain radiation pattern, SAR restrictions, and link communication performances are investigated. Section V shows a comparison of the proposed antenna performances with those of recently published implantable antennas and Section VI summarizes the main results.

## II. ANTENNA DESIGN AND OPTIMIZATION

### A. Antenna structure

The side view and 3D view of the proposed antenna are represented in Figures 1 (a) and (b), respectively. The antenna is fed by a coaxial cable using a sub-miniature version A (SMA) connector with a characteristic impedance of  $50 \Omega$  and inner radius of  $0.63$

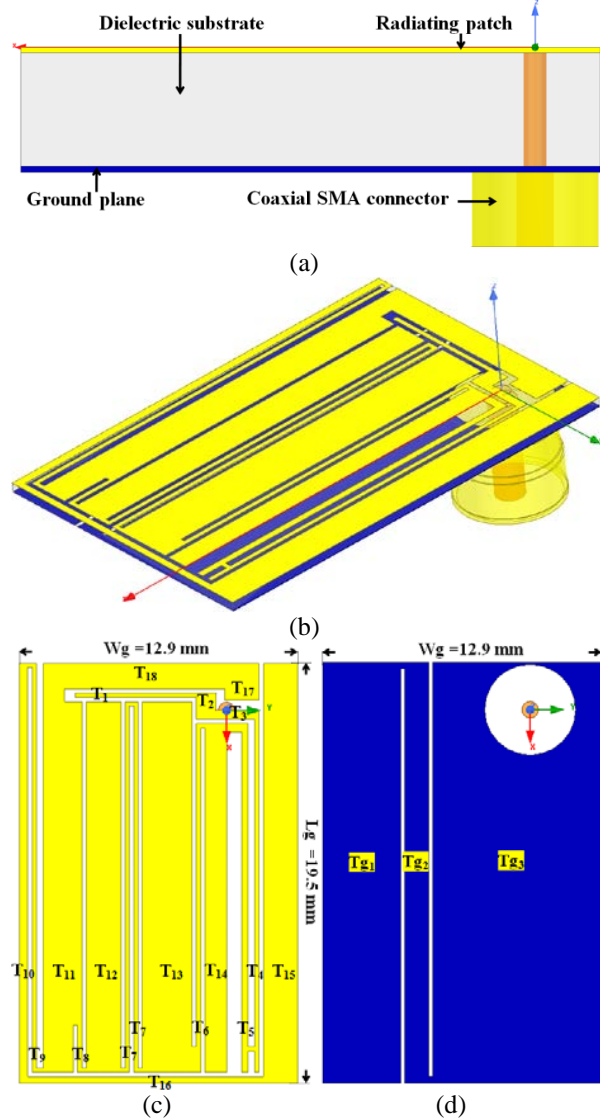


Fig. 1. The proposed antenna. (a) Side view. (b) 3D view. (c) Top view. (d) Ground plane.

Table 1: Various shaped patch tracks  $T_i$ , and sub-tracks  $ST_j$ , ground plane tracks  $Tg_k$ , and sub-tracks  $STg_l$  dimensions

Tracks and sub-tracks number	Dimensions [mm × mm]	Tracks and sub-tracks number	Dimensions [mm × mm]
$T_1$	$0.2 \times 5.6$	$ST_1 (T_4 - T_5)$	$0.2 \times 0.3$
$T_2$	$1.2 \times 0.9$	$ST_2 (T_5 - T_{14})$	$0.4 \times 0.7$
$T_3$	$0.4 \times 2.0$	$ST_3 (T_{14} - T_6)$	$0.2 \times 0.2$
$T_4$	$0.2 \times 16.4$	$ST_4 (T_6 - T_{13})$	$1.2 \times 0.2$
$T_5$	$0.3 \times 16.2$	$ST_5 (T_{13} - T_7)$	$0.2 \times 0.2$
$T_6$	$0.2 \times 15.6$	$ST_6 (T_7 - T_7)$	$0.2 \times 0.2$
$T_7$	$17.2 \times 0.2$	$ST_7 (T_7 - T_{12})$	$0.2 \times 0.2$
$T_8$	$17.2 \times 0.2$	$ST_8 (T_{12} - T_8)$	$0.2 \times 0.2$
$T_9$	$19.0 \times 0.2$	$ST_9 (T_8 - T_{11})$	$0.2 \times 12.0$
$T_{10}$	$19.0 \times 0.4$	$ST_{10} (T_{11} - T_9)$	$0.2 \times 0.3$
$T_{11}$	$17.2 \times 1.4$	$ST_{11} (T_9 - T_{10})$	$0.2 \times 0.2$
$T_{12}$	$17.2 \times 1.6$	$ST_{12} (T_{11} - T_{18})$	$1.0 \times 0.6$
$T_{13}$	$17.2 \times 2.3$	$Tg_1$	$19.5 \times 3.6$
$T_{14}$	$16.2 \times 1.0$	$Tg_2$	$19.5 \times 1.1$
$T_{15}$	$19.5 \times 1.6$	$Tg_3$	$19.5 \times 7.8$
$T_{16}$	$0.3 \times 10.9$	$STg_1 (Tg_1 - Tg_2)$	$0.3 \times 0.2$
$T_{17}$	$1.7 \times 1.6$	$STg_2 (Tg_2 - Tg_3)$	$0.3 \times 0.2$
$T_{18}$	$1.2 \times 8.4$		

mm. The all-compact structure is covered with a thin layer of the polymer parylene-C (relative permittivity  $\epsilon_r = 2.95$ , loss tangent  $\tan\delta = 0.013$ , and thickness =  $20 \mu\text{m}$ ) to guarantee the biocompatibility and the electrical isolation. Herein, the planar conductors consist of copper with thickness  $18 \mu\text{m}$  and conductivity  $\sigma = 58 \text{ MS/m}$ .

The antenna consists of three parts from the top to bottom: shaped patch with slotting, Cufion substrate, and open-end slotted ground plane.

**Part 1, the radiating patch:** A detailed description of the antenna radiating shaped patch is given by Figure 1(c), where the radiating patch consists of 18 tracks  $T_i$  ( $i = 1, \dots, 18$ ) obtained by slotting, and their optimized dimensions are given in Table 1. The various tracks are connected between them using a set of sub-tracks  $ST_j$  ( $T_{i1} - T_{i2}$ ) of total number 12. The particular case of the sub-track occurred between tracks 4 and 5 and is located at a distance  $1.2 \text{ mm}$  from the track  $T_{16}$ .

**Part 2, the dielectric substrate:** A low permittivity and very low loss substrate is used, Cufion with relative permittivity  $\epsilon_r = 2.05$ , loss tangent  $\tan\delta = 0.00045$ , and dielectric thickness  $Thd = 0.38 \text{ mm}$ . In addition to these frequency-uniform electrical properties [41], this substrate is relatively flexible, which allows freedom of the muscle movement and avoids injuries caused by sharp edges.

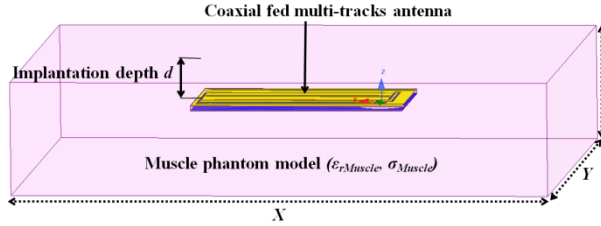


Fig. 2. 3D view of the implanted antenna in the muscle phantom model  $(X, Y, Z) = (110, 115, 25)$  mm.

**Part 3, the ground plane:** It consists of three tracks  $Tg_k$  ( $k = 1, 2, 3$ ) and two sub-tracks  $STg_1$  ( $Tg_1 - Tg_2$ ), and  $STg_2$  ( $Tg_2 - Tg_3$ ) as shown in Figure 1 (d). The ground plane tracks and the sub-track dimensions are also given in Table 1.

### B. Structure of the phantom model

For implantation, a single layer muscle human tissue phantom model is used, where the whole antenna is submerged in the phantom center at a distance  $d = 4$  mm as shown in Figure 2. The phantom has a parallelepiped form of dimensions 110, 115, and 25 mm along the axes  $X$ ,  $Y$ , and  $Z$ , respectively.

The dielectric properties of human tissues are frequency-dependent as demonstrated by the model of Gabriel *et al.* [42]. Herein, the model is implemented to generate the frequency-dependent conductivity and relative permittivity of the muscle, fat, and skin; the data are represented in Figure 3 for interest frequencies.

Fat and skin generated data will be used in Section III for studying tissues and implantation depth effects on implanted antenna performances.

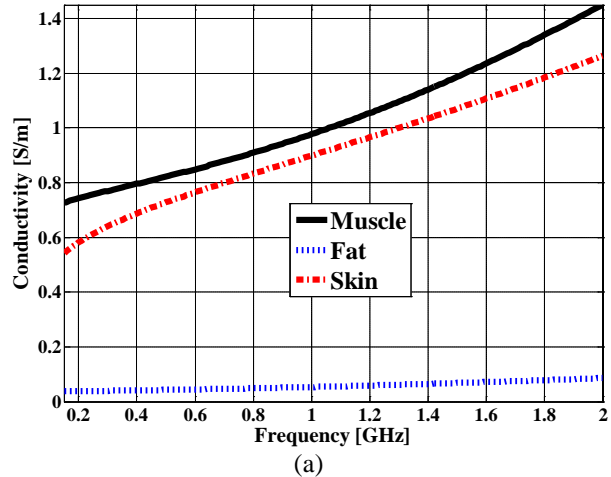
### C. Design process

It is not a quiet simple task to derive an exact straightforward theoretical model for the analysis and design of the proposed multi-track antenna, due to the complex form of its radiating element with irregular shape. Thus, we should make recourse to rigorous numerical methods.

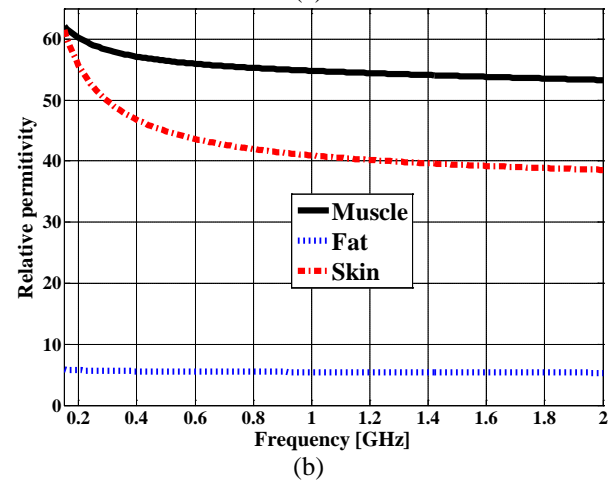
To design, simulate and solve the corresponding electromagnetic problem, in a heterogeneous, complex, and non-uniform structure, the Ansys<sup>®</sup> HFSS, which is based on 3D full-wave finite element method (FEM) field solver is used.

Since our objective is to obtain closely multi-band operation for telemetry, we perform two techniques: 1) current path lengthening by inserting a slot in the radiating patch and 2) embedded open-end slots in the ground plane.

Now, the design procedure of the proposed implantable multi-track antenna is outlined. The design is accomplished in four steps by inserting slots in the



(a)



(b)

Fig. 3. Dielectric properties of the muscle, fat, and skin human tissues. (a) Conductivity  $\sigma$  [S/m]. (b) Relative permittivity  $\epsilon_r$ .

radiating patch and open-end slots in the ground plane as shown in Figure 4. The corresponding reflection coefficients calculated with the antenna submerged at a distance  $d = 4$  mm in the muscle phantom model were used to carry out the design (Figure 5).

**[Step#1:]** Start from an initial non-optimized design in which a microstrip antenna with full ground plane, where the antenna feed is fixed at the origin of the coordinate system as shown in Figure 4 (a). The dimensions are those of Figure 1 (c):  $L_g \times W_g = 19.5 \times 12.9$  mm<sup>2</sup>. From the results shown in Figure 5, step#1, it is seen from the computed reflection coefficient that the antenna does not resonate in the frequency band of interest (dc-2 GHz).

**[Step#2:]** Insert a meandered slot with variable sections of a minimum width; for example, 0.2 mm, in the radiating patch as shown in Figure 4 (b). This creates four resonance frequencies, as shown by the corresponding reflection coefficient. The impedance matching in this

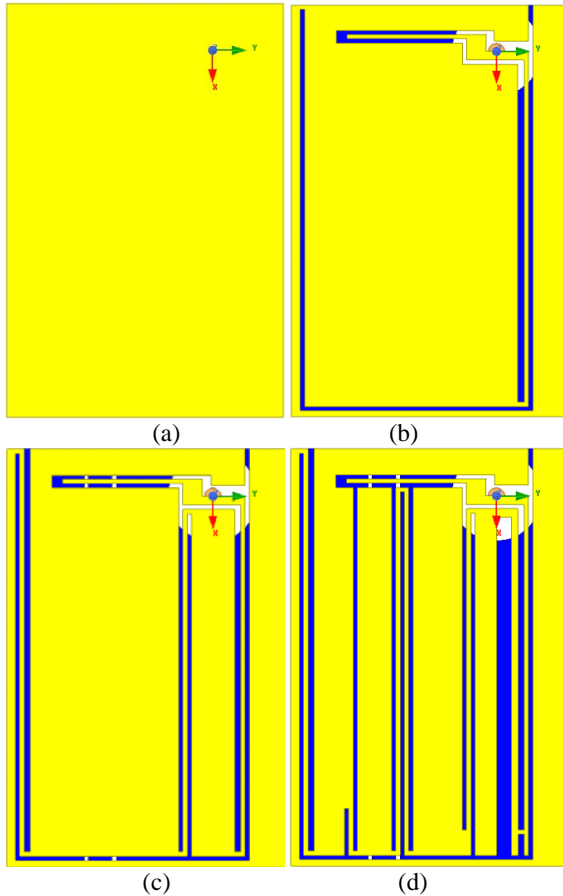


Fig. 4. Representation of the evolution of the patch and ground plane shapes with the four-step design process: (a) step #1; (b) step #2; (c) step #3; (d) step #4.

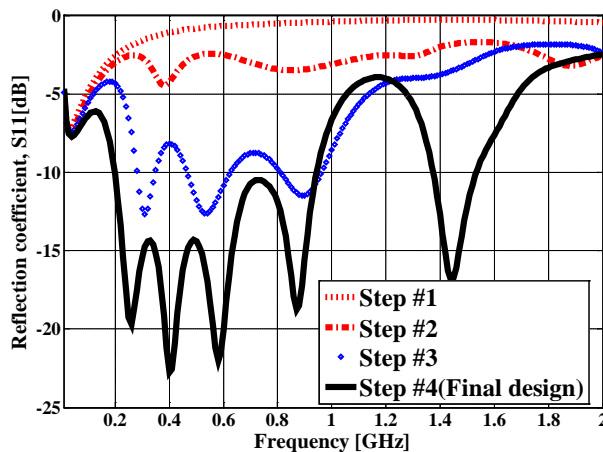


Fig. 5. The reflection coefficients ( $S_{11}$ ) corresponding to the design process steps.

step is poor for the all created resonance frequencies as shown in Figure 5, step #2.

**[Step#3:]** The poor matching obtained in step #2 is improved for the first three resonances by inserting three other slots in parallel to the edges of the meandered slot introduced in the previous step as represented by Figure 4 (c). Also, the remaining fourth resonance frequency is shifted considerably to low without reaching its final target resonance frequency. For the fourth resonance frequency impedance matching enhancement, two parallel open-end slots are inserted in the ground plane. The reflection coefficient corresponding to this step is shown clearly in Figure 5, step #3.

**[Step#4:]** The poor obtained matching is reinforced again by inserting five other slots in the middle of the radiating patch, and another slot in parallel to the right edge of the meandered slot inserted before in step #2, as shown Figure 4 (d). A further shifting of the four resonance frequencies to their targeted counterparts is obtained with closer resonances. A fifth resonance frequency has been added in high frequencies. Finally, for resonance frequency tuning, adjustment of slots dimensions is performed. Results relative to reflection coefficient of this step are reported in Figure 5, step #4.

This marks the end of the antenna design and optimization. The final design yields a total impedance bandwidth of 0.90 GHz (0.20–0.94 and 1.37–1.53 GHz), and the obtained reflection coefficients ( $S_{11}$ ) are  $-22.91$ ,  $-18.46$ ,  $-18.06$ ,  $-18.65$ ,  $-11.61$ ,  $-12.08$ , and  $-16.68$  dB at frequencies 403, 433, 611, 868, and 928 MHz and 1.395 and 1.432 GHz, respectively.

At this stage, we would say a word on the computation time. It is found that the computation time is highly depending on the antenna complexity which is directly related to the number of tracks of the radiating antenna. Hence, the computation time increases with the step number in the design process, detailed above in Section II-C. Later, in the simulations carried out in Section IV, computation time will increase again when the antenna is implanted in a realistic human model.

#### D. Ground plane open-end slotting effect

Figure 6 presents a comparison of the reflection coefficients of the final design with and without open-end slots inserted in the ground plane.

The open-end slots inserted in the ground plane enhance considerably the impedance bandwidth in higher frequencies. Otherwise, considering it is reported that an implantable antenna with full ground plane is preferred in some WIMDs, the designed antenna with full ground plane is still effective especially for the lower part of the targeted frequencies and remains a good candidate for such systems.

#### E. Free space measurements

To verify the performance of the designed implantable antenna in free space, a prototype of

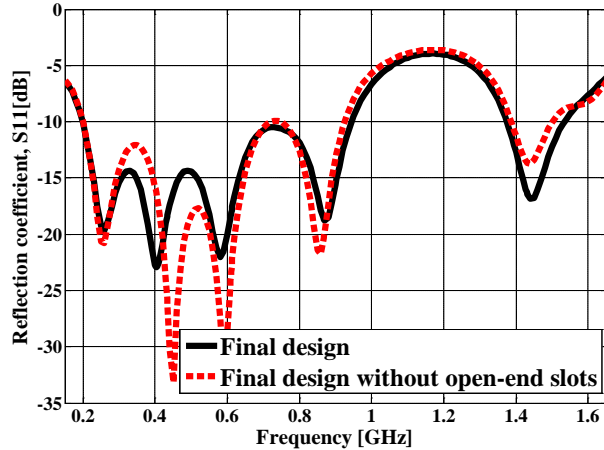


Fig. 6. Ground plane open-end slotting effect on impedance bandwidth enhancement.

the antenna was fabricated and appropriate measurement setup was used. A top and bottom view of the fabricated antenna and the measurement setup are shown, respectively, in Figures 7 (a) and (b).

The antenna consists of a coax-feed double-sided patch printed on a low permittivity and very low loss Cufion substrate, with the same dielectric properties and thickness used in the simulation. A professional milling machine combined with high-precision  $45^\circ$  milling tools are used to engrave both the radiating patch and the ground plane. The antenna was connected to the vector network analyzer (VNA). A coaxial probe with an SMA connector that presents a characteristic impedance of  $50 \Omega$  is used to feed the antenna. Figure 8 displays a comparison of the measured and simulated return loss in free space.

Obviously, the antenna is not efficient in air, but according to the figure, we can see that numerical and experimental results are in a very good agreement. The measured resonance frequencies correspond to those predicted by the simulation, indicating that all current paths are present.

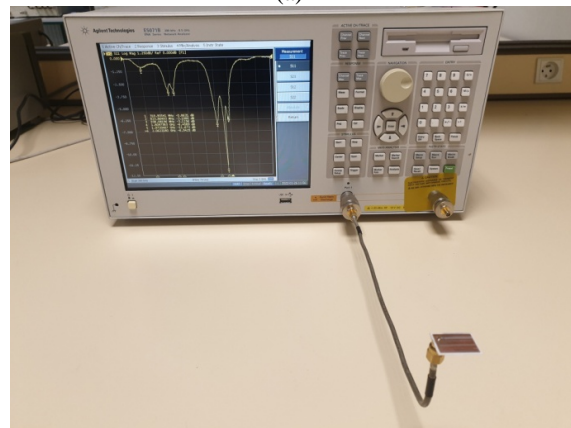
### III. TISSUES AND IMPLANTATION DEPTH EFFECTS

In realistic implantation, the antenna is surrounded by various tissues that present different dielectric properties. The dielectric properties of all biological human tissues are frequency dependent. Examples of such characteristics are given for the muscle, fat, and skin in Figure 3 and will be used throughout this section. Furthermore, some types of tissues, such as the fat, possess variable thickness. To predict accompanied effects, simulations are performed into two main stages.

The first stage consists of one layer tissue with a total volume of  $110 \times 115 \times 25 \text{ mm}^3$  in which the



(a)



(b)

Fig. 7. (a) Fabricated antenna. (b) Measurement setup.

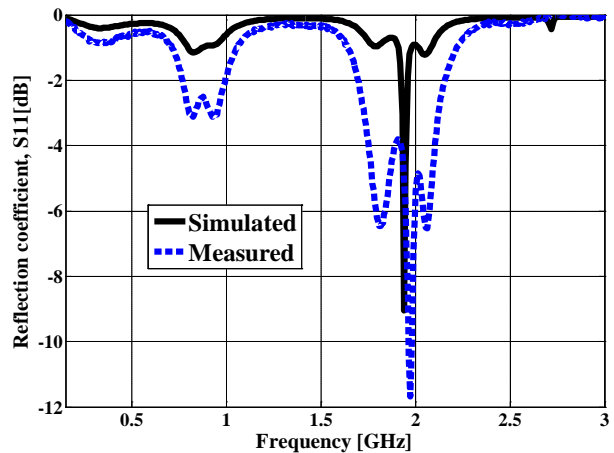


Fig. 8. Measured and simulated reflection coefficients ( $S_{11}$ ) in air.

antenna implantation depth  $d_{oT}$  is set to 4 mm as shown in Figure 9 (a). Two different layers, skin and fat, are considered and the corresponding reflection coefficients

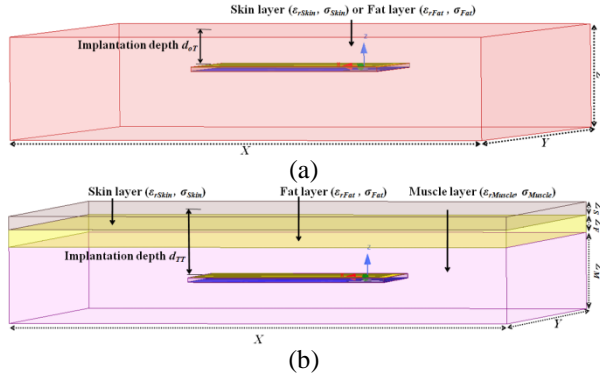


Fig. 9. Layered models used for tissues and depth effects study. (a) The one layered phantom model: skin or fat  $(X, Y, Z) = (110, 115, 25)$  mm. (b) The three layered phantom model: skin  $(X, Y, Z) = (110, 115, Z_S)$  mm, fat  $(X, Y, Z) = (110, 115, Z_F)$  mm, and muscle  $(X, Y, Z) = (110, 115, Z_M)$  mm.

Table 2: Various studied scenarios of a three-layer phantom model together with their physical dimensions

Scenario	Layers thickness, and implantation depth [mm]	Implantation tissue
1	$Z_S = 1.3, Z_F = 1.7, Z_M = 22.0, d_{TT} = 4.0$	Muscle
2	$Z_S = 1.3, Z_F = 1.7, Z_M = 22.0, d_{TT} = 6.5$	
3	$Z_S = 2.0, Z_F = 10.0, Z_M = 13.0, d_{TT} = 15.0$	
4	$Z_S = 1.3, Z_F = 1.7, Z_M = 22.0, d_{TT} = 0.6$	Skin
5	$Z_S = 2.0, Z_F = 10.0, Z_M = 13.0, d_{TT} = 1.5$	

are compared in Figure 10 to the one previously calculated in muscle layer. Results show that fat introduces an important shift of the resonance frequencies to higher frequencies due to lower values of relative permittivity of this human tissue layer and impedance mismatching is observed especially at lower frequencies. On the contrary, skin tissue layer introduces small modifications since it presents a closer permittivity with muscle.

The second stage consists of three layer tissues: muscle, fat, and skin, whose thicknesses are  $Z_M, Z_F$ , and  $Z_S$ , respectively, as shown in Figure 9 (b). The antenna implantation depth  $d_{TT}$ , in the layer of muscle, is defined as the distance between the radiating patch surface and the most close air–skin interface. Five scenarios corresponding to different values of implantation depth and layers thicknesses are given in Table 2 and are simulated. The whole volume of the structure is kept  $110 \times 115 \times 25$  mm<sup>3</sup> as in the first stage.

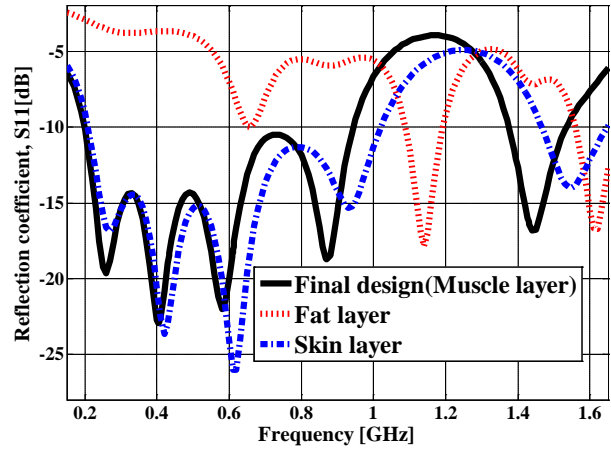


Fig. 10. Reflection coefficients ( $S_{11}$ ) in one layer tissue phantom model.

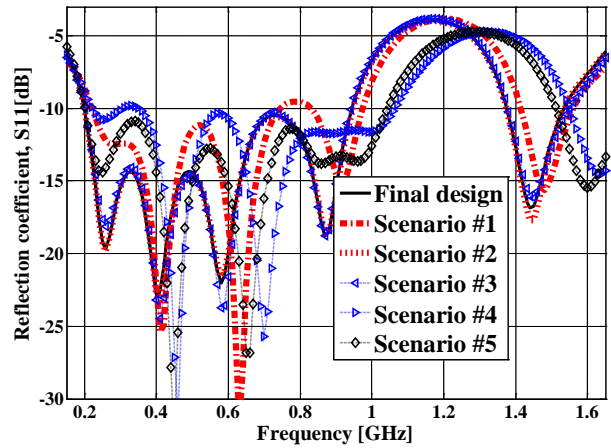


Fig. 11. Reflection coefficients ( $S_{11}$ ) in a three-layer tissues phantom model.

From the return loss results of the second stage scenario #1 given in Figure 11, we note that the use of three-layer human tissues phantom model shifts all implanted antenna resonance frequencies to higher frequencies with respect to the implantation in one layer muscle phantom model. Despite this shift, due to a lower permittivity of the media, a good impedance matching is maintained.

The obtained results of scenarios #2 and #3 presented in Figure 11 show that an appropriate increase in the implantations depth  $d_{TT}$  in the muscle allows reaching back the target resonance frequencies with very fine impedance matching level.

Furthermore, the designed skin implanted antenna of scenarios #4 and #5 present a good impedance matching for almost all target frequencies which are in this case, the MedRadio band (401–406) MHz, the ISM bands (433.1–434.8), (868.0–868.6), and

(902.8–928.0) MHz, and the Wireless Medical Telemetry Service (WMTS) band (608–614) MHz. The obtained results shown by scenarios #2, #3, #4, and #5 are in agreement with those presented by Lee *et al.* [43], where a skin- and muscle-implanted broadband PIFA antenna has been proposed for communication in the MICS band (402–405) MHz.

#### IV. ANTENNA OPERATION IN PRACTICAL IMPLANTATION

The proposed antenna is intended to be implanted in the muscles of the human body. To this end, two implantation tests have been simulated using the realistic human model of VHP-Female version 2.1 (age of 60 years old, height of 162 cm, and weight of 88 kg) of NEVA Electromagnetics, LLC [44]. This full body computational model of real human anatomy is constituted of 25 individual tissues distributed in 203 tissue parts. All inner tissues and organs are contained by the average body shell which is assigned as muscle tissue surrounded by fat and skin shells. For more accuracy, the individual dielectric properties of tissues [42] are used. Figure 12 shows two antenna implantation testing in the underneath the scalp (e.g., intracranial pressure monitoring) and in the upper arm muscle (e.g., blood pressure monitoring, and transcutaneous glucose monitoring). The antenna is implanted in the average body tissue at a depth of 5 and 11 mm from the close air–skin tissue surface for the first and the second implantation testing, respectively.

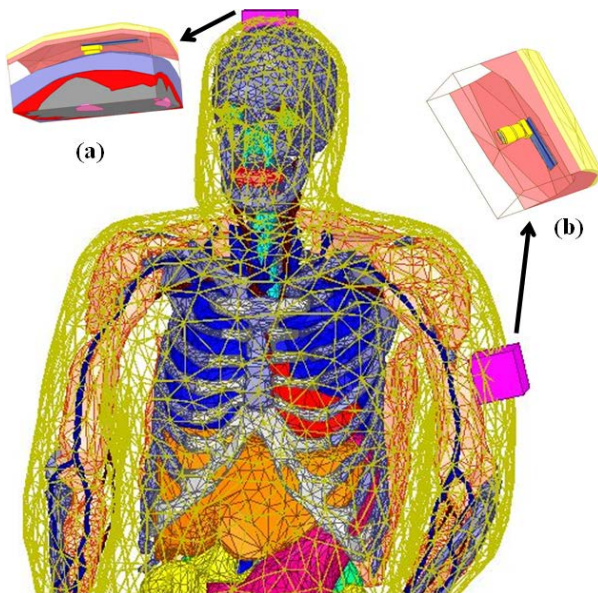


Fig. 12. Practical antenna implantation: (a) in the underneath the scalp; (b) in the upper arm.

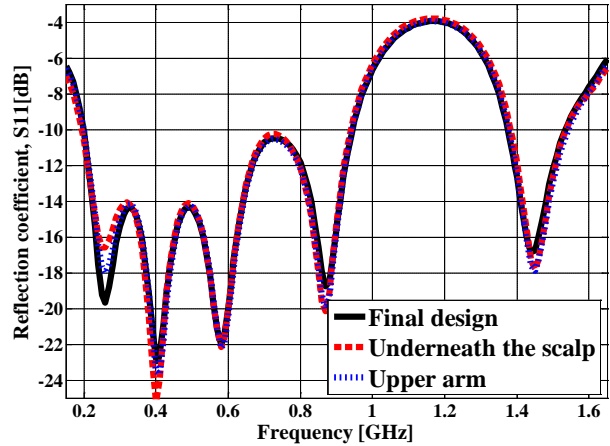


Fig. 13. Simulated reflection coefficients ( $S_{11}$ ) of the antenna implantation tests in a realistic human body model.

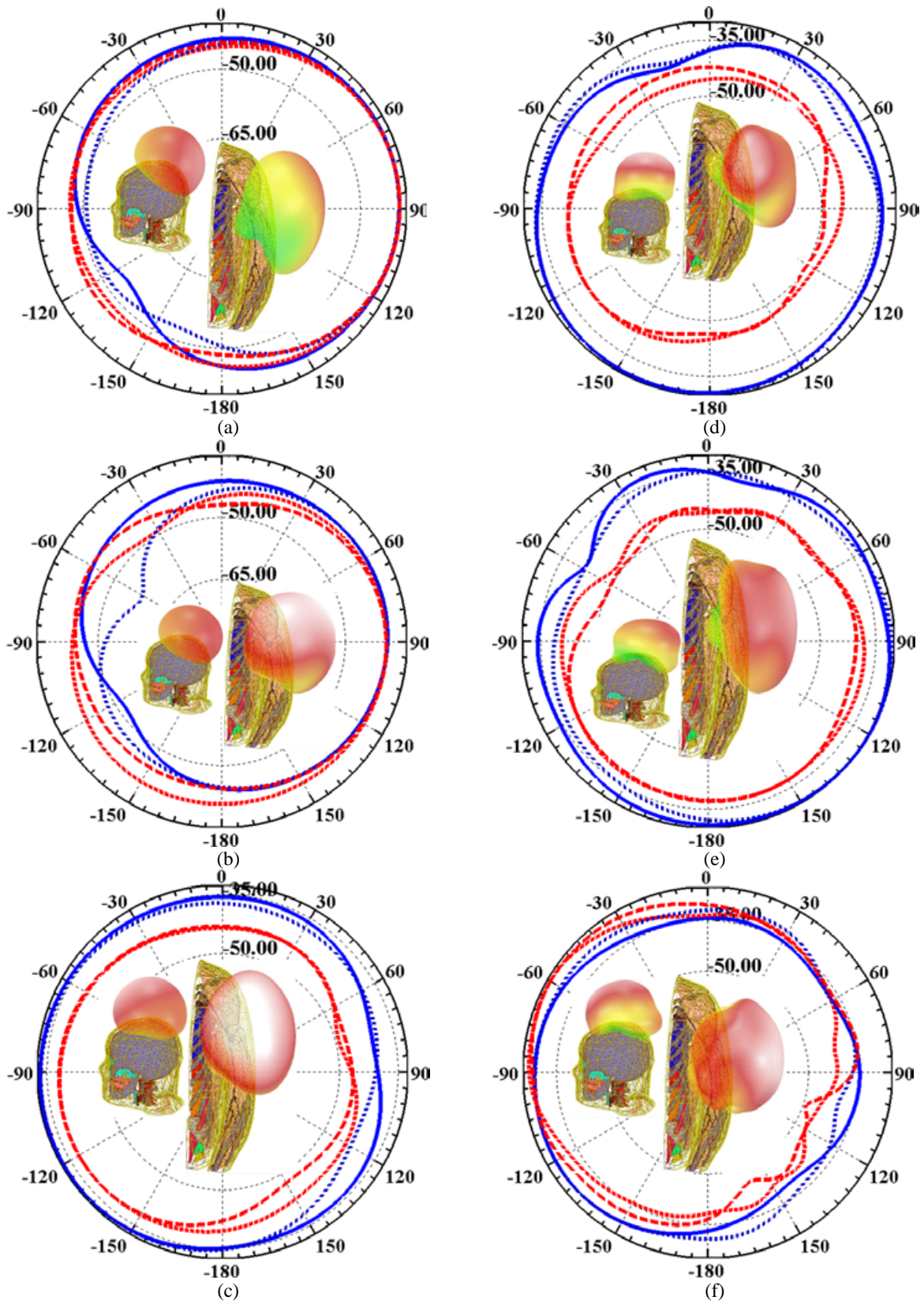
##### A. Reflection coefficients

The simulated reflection coefficients of the two tests implantations are given in Figure 13, along with that of the final design already presented in Section II. Comparison of impedance bandwidth results shows that: 1) in the underneath the scalp implantation, the lower wideband (0.19–0.94) GHz is widened by 10 MHz toward lower limit bound, whereas the higher frequency band (1.38–1.54) GHz is shifted by 10 MHz toward upper limit bound, and 2) in the upper arm implantation, the impedance bandwidth of the lower wideband remains the same as the final design, whereas the impedance bandwidth of the higher band coincides with the underneath the scalp implantation. Thus, the exhibited total impedances bandwidth is of 0.91 and 0.90 GHz in the underneath the scalp and in the upper arm antenna implantation, respectively.

##### B. Far-field gain radiation pattern

An implanted antenna must be able to ensure communication requirements between the WIMDs and the external gateway/base-station. Thus, it is essential to obtain sufficient radiation power from the antenna implanted within the body. Figures 14 (a)–(g) present the simulated 3D far-field gain radiation patterns obtained for the two previous implantations together with the corresponding 2D far-field gain radiation patterns in  $E$  and  $H$  planes.

The corresponding values of the peak gain obtained in the underneath the scalp antenna implantation are  $-41.55$ ,  $-39.58$ ,  $-32.97$ ,  $-30.52$ ,  $-30.09$ ,  $-27.69$ , and  $-27.35$  dB. For in the upper arm, the corresponding values are  $-41.51$ ,  $-40.00$ ,  $-37.53$ ,  $-41.05$ ,  $-36.99$ ,  $-25.93$ , and  $-25.24$  dB at frequencies 403, 433, 611, 868, and 928 MHz and 1.395 and 1.432 GHz, respec-

Fig. 14. *Continued.*

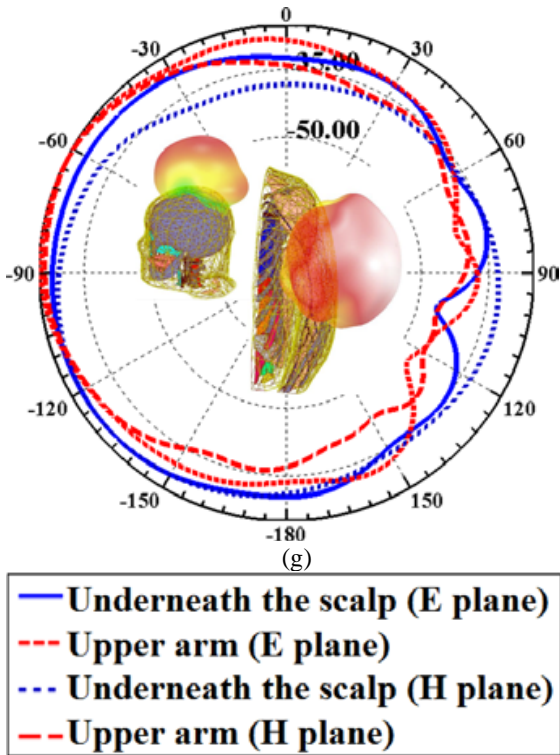


Fig. 14. Simulated 2D ( $E$  and  $H$  planes), and 3D far-field gain radiation patterns of antenna implantation tests in the underneath the scalp and in the upper arm at frequencies: (a) 0.403, (b) 0.433, (c) 0.611, (d) 0.868, (e) 0.928, (f) 1.395, and (g) 1.432 GHz.

tively. Note that, for both antenna implantation tests, the main radiated power is distributed toward the almost directions of the off-body environment.

This is valid for the all considered operating frequencies. Thus, the radiation characteristics of the proposed antenna are able to produce an effective wireless communication links between the interior and the exterior of the body. Besides, by comparison with the peak gain values obtained in the final design, a gain decreasing the overall considered frequency is observed. A maximum decrease of peak gain of 5 dB is noticed at the frequency 403 MHz. The decrease is probably due to the implantation depths and losses presented by the conductivity of the heterogeneous implantation testing mediums.

### C. Safety considerations and electromagnetic interference

The patient safety is in priory. To this end, the general public exposure is restricted by IEEE C95.1-1999 and IEEE C95.1-2005 standards, in which the two limitations 1g averaged SAR  $\leq 1.6$  W/kg [45], and 10 g averaged SAR  $\leq 2$  W/kg [46] must be respected, respec-

Table 3: Calculate maximum SAR values and corresponding permitted power

Model	Freq. [GHz]	Max SAR [W/kg]		Max net-input power [mW]	
		1 g-avg	10 g-avg	1 g-avg	10 g-avg
In the underneath the scalp	0.403	555.95	87.55	2.87	22.84
	0.433	563.44	86.65	2.83	23.08
	0.611	636.57	88.29	2.51	22.65
	0.868	624.63	90.53	2.56	22.09
	0.928	579.50	84.02	2.76	23.80
	1.395	599.58	81.31	2.66	24.59
	1.432	575.72	84.69	2.77	23.61
In the upper arm	0.403	554.54	89.57	2.88	22.32
	0.433	562.64	88.94	2.84	22.48
	0.611	635.47	89.97	2.51	22.22
	0.868	616.31	90.74	2.59	22.04
	0.928	571.37	84.44	2.80	23.68
	1.395	584.13	81.35	2.73	24.58
	1.432	547.41	83.84	2.92	23.85

tively. Hence, the power incident to an implantable antenna should not exceed the corresponding value for each limitation. Assuming that the net-input power of the antenna is set to 1 W for the two practical implantation tests simulated previously in this section, the maximum 1-g averaged and 10-g averaged SAR and the corresponding maximum allowed net-input power values are listed in Table 3.

Moreover, to mitigate EM interference with nearby services, the effective isotropic radiated power (EIRP) of a transmitter antenna is limited as mentioned by the following equation:

$$\text{EIRP}[\text{dBm}] = P_{\text{in}}[\text{dBm}] + G[\text{dBi}] \leq \text{EIRP}_{\text{max}}[\text{dBm}], \quad (1)$$

where  $P_{\text{in}}$  is the net-input power, and  $G$  is the radiation gain of the antenna. The implanted antenna in transmitting serve the up-link, and the  $\text{EIRP}_{\text{max}}$  is set to  $-16$ ,  $7.85$ ,  $10.8$ ,  $11.85$ ,  $36$ ,  $22.2$ , and  $22.2$  dBm for frequencies 403, 433, 611, 868, and 928 MHz and 1.395 and 1.432 GHz, respectively [5, 22, 47].

The implanted antennas exhibit low gain values. Thus, the maximum net-input power remains limited by the SAR restrictions. For the two simulated implantation tests, the calculated value of the net-input power of 4 dBm (2.51 mW) allows to meet the patient safety restrictions of both the most (1-g averaged SAR  $\leq 1.6$  W/kg and less (10-g averaged SAR  $\leq 2$  W/kg) limitations of IEEE standards, and this is validated for all considered frequencies. In addition, this value is much greater than the limit of the input power of the implantable antennas, which is  $25 \mu\text{W}$  [24, 29, 32, 34, 37].

Table 4: Parameters description of the link margin calculation

Transmission		
Freq [GHz]	Operating frequency	0.403, 0.43, 0.611, 0.868, 0.928, 1.395, 1.432
$P_{Tx}$ [dBW]	Tx power	-46
$G_{Tx}$ [dBi]	Tx antenna gain	Max gain (free space), mean gain (indoor)
$L_{Txf}$ [dB]	Tx feeding loss	0
$L_{Txm}$ [dB]	Tx impedance mismatch loss	0.3
$L_{pol}$ [dB]	Polarization mismatch loss	2
Propagation scenarios		
$LP_m$ ( $m = 2$ ) [dB]	Free space	Path-loss exponent $m$ and distance dependent
$LP_m$ ( $m = 1.5$ ) [dB]	Indoor LOS	
$LP_m$ ( $m = 3$ ) [dB]	Indoor NLOS	
$dL$ [m]	Tx-Rx distance	To be calculated
$d_0$ [m]	Reference distance	1
$\lambda$ [m]	Wavelength in free space	$(3 \times 10^8)/\text{Freq}$
$\chi_\sigma$ [1]	Shadowing factor	0
Receiver		
$G_{Rx}$ [dBi]	Rx antenna gain	2.15
$L_{Rxf}$ [dB]	Rx feeding loss	0
$L_{Rxm}$ [dB]	Rx mismatch loss	0
$T_o$ [K]	Ambient temperature	293
$k$ [1]	Boltzmann const.	$1.38 \times 10^{-23}$
$NF$ [dB]	Receiver noise figure	3.5
$N_o$ [dB/Hz]	Noise power density	-199.95
Signal quality		
$B_r$ [bps]	Bit rate	$100 \times 10^3$
BER [1]	Bit error rate	$1.0 \times 10^{-5}$
$E_b/N_o$ [dB]	Ideal-PSK, ideal-BPSK	9.6
$G_c$ [dB]	Coding gain	0
$G_d$ [dB]	Fixing deterioration	2.5

#### D. Link communication performances

The link budget calculation allows evaluating the far-field communication link quality. It allows evaluating the communication performances between the WIND antenna and the exterior gateway/base-station for envisaged communication requirements with including various transmission constraints. The link established between the transmitter designed antenna Tx and an exterior receiver antenna Rx is evaluated. The link margin (LM) is given as a function of the carrier to noise power density ratio ( $C/N_0$ ) as detailed by the following equation [2, 20, 22]:

$$LM = \text{Link} \frac{C}{N_0} - \text{Required} \frac{C}{N_0} = (P_{Tx} + G_{Tx} + G_{Rx} - L_{Txf} - L_{Txm} - LP_m - L_{pol} - L_{Rxf} - L_{Rxm} - N_0) - \left( \frac{E_b}{N_0} + 10 \log_{10} B_r - G_c + G_d \right), \quad (2)$$

where

$$LP_m = 10m \log_{10} \left( \frac{dL}{d_0} \right) + 20 \log_{10} \left( \frac{4\pi d_0}{\lambda} \right) + \chi_\sigma, \quad (3)$$

and

$$N_0 = 10 \log_{10}(kT_o(NF - 1)). \quad (4)$$

Various parameter descriptions and their values used for LM calculation are listed in Table 4. The available transmitter power  $P_{Tx}$  is set to 25  $\mu$ W and the transmitter gain  $G_{Tx}$  values considered are those obtained in the first practical test as described in Section IV-B. The considered receiver antenna is a well matched dipole antenna with impedance mismatch loss  $L_{Rxm}$  equal to 0 dB and gain  $G_{Rx}$  equal to 2.15 dB [22]. Also, the impedance mismatching loss  $L_{Txm}$  of the transmitter antenna is set to 0.3 dB, which is the maximum value calculated for all considered frequencies. The feeding losses  $L_{Txf}$  and  $L_{Rxf}$  of the transmitter and the receiver, respectively, are neglected. In addition, the obtained polarization is almost linear; thus, the polarization mismatch loss  $L_{pol}$  is taken 2 dB [11].

Three different propagation scenarios are considered to account for the propagation channel effects: (1) in the free space, (2) in the indoor line-of-sight (LOS), and (3) in the indoor non-line-of-sight (NLOS). To this end, the most suitable model of log-distance for the indoor loss estimation is used. For the first scenario communication channel, the transmitter gain  $G_{Tx}$  values are those simulated maximum values, whereas for the indoor channels, i.e., LOS and NLOS, the mean gains are more suitable [22] and their simulated values are considered for the LM calculation.

The shadowing factor  $\chi_\sigma$  is neglected and the reference distance  $d_0$  is set as 1 m for all three propagation scenarios. The signal quality parameter of the bit rate  $B_r$  is chosen to cover largely the requirements of the

clinical applications associated with practical tests simulated in Section IV. For example, the bit rate for the subcutaneous glucose sensor, and the intracranial pressure transmission is less than 10 kbps [4], and is of 7 kbps [29, 32, 37], respectively.

The other receiver Rx and signal quality parameter values adopted are those of references [2, 20]. These other signal quality parameter values are agreed from several WIMDs. The data communication between a transmitter and a receiver antennas remains possible when the  $LM > 0$  dB. Figure 15 illustrates the LM values calculated in function of transmitter–receiver distance  $dL$  for the three propagation scenarios.

The communication distances offered by the indoor LOS channel communication are larger than those obtained in the free space and in the indoor NLOS environments.

Due to the lack of LOS, the LM decrease is rapid in the indoor NLOS environments, which leads to low possible communication distance. Nevertheless, this distance communication remains sufficient in all the three channels. In the free space, the communication distance starts from 19 m at 403 MHz to reach 33.5 m at 611 MHz, and in the indoor LOS propagation scenario, the communication distance begins from 14 m at 403 MHz until and 45m at 868 MHz, and although the indoor NLOS is a rigorous propagation scenario, the communication can be established from the distance of 3.75 m at 433 MHz to 6.5 m at 868 MHz. Thus, the telemetry communication links between the proposed implantable antenna and an exterior gateway/base-station can be established in both the free space and in the indoor environments with practical distances.

## V. COMPARISON WITH RECENTLY PUBLISHED IMPLANTABLE ANTENNAS

The performances of the proposed multi-track implantable antenna are compared with data brought from the literature. Various targeted operating frequency bands are considered for this comparison. The results are reported in Table 5.

Thanks to an efficient design combined with using a low permittivity substrate, the proposed antenna exhibits both low volume and broadband behavior. In addition, as it does not require any superstrate, the proposed configuration presents a very low thickness. Actually, the proposed antenna covers several telemetry frequencies with large available frequency bands, whereas voluminous antennas covering less number of operating frequency bands are noticed, as reported in published studies. Note that our obtained peak gain values are very near to those available from the literature in almost all

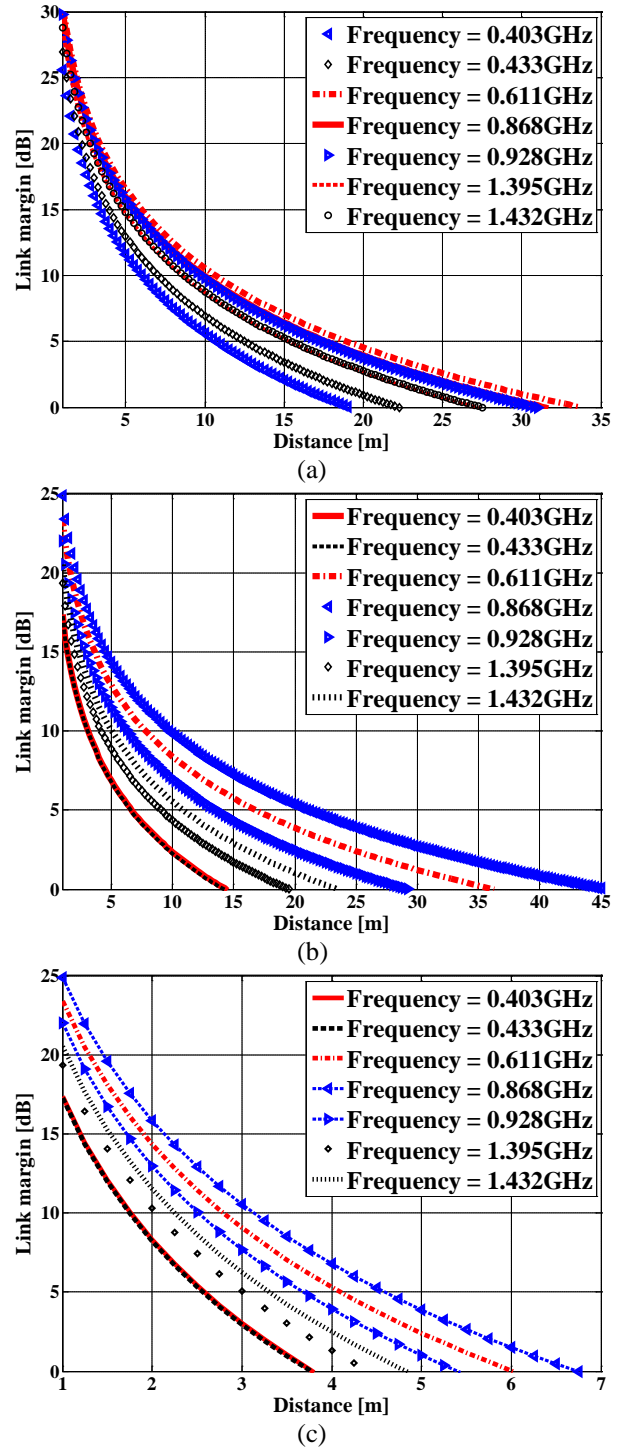


Fig. 15. Link margin LM calculation: (a) free space loss; (b) indoor LOS loss; (c) indoor NLOS loss.

cases. Note also that the obtained SAR values are very comparable to those in the literature with improvements in some cases and small degradation in other cases.

Table 5: Comparison of the designed antenna performances with those of previous proposed implantable antennas from the literature

Ref.	Volume [mm <sup>3</sup> ]	Available bands [MHz]	Freq. [MHz]	Peak gain/ realized gain [dBi]	Max. SAR [W/kg] [input power = 1 W]		Substrate/ superstrate ( $\epsilon_r, \tan\delta$ )	Total thickness [mm]	
					1-1999 1g-avg	1-2005 10g-avg			
					[13]	560			360
[22]	203.4		27	402	G. -36.9	324	66.6	Both: RO3210 (10.2, 0.003)	1.8
			28	433	G. -35.9	309	66.3		
			38	868	G. -35.1	297	66.0		
			40	915	G. -32.9	295	67.5		
[27]	248.92		100	402	G. -46	338	—	Both: RO3010 (10.2, -)	1.27
			300	2440	G. -19	482	—		
[32]	52.5		64	405	G. -40.8	665	93.2	Both: Rogers 6010 (10.2, 0.0035)	0.5
			91	915	G. -32.9	837	93.9		
			105	2450	G. -22.3	759	87.2		
[34]	21		80	915	G. -26.4	380	40.4	Both: RT/duroid 6010 (10.2, 0.0035)	0.5
			115	1900	G. -23	358	38.2		
			180	2450	G. -20.47	363	40.3		
[36]	254		150	401	G. -22	—	39.1	Both: RO3210 (10.2, 0.003)	2.45
				433	G. -23	—	39.5		
			52	1427	G. -17	—	58.7		
			102	2400	G. -16	—	76.8		
[37]	17.15		148	402	G. -30.5 G. -30	588	544	Both: RT/duroid 6010 (10.2, 0.0035)	0.377
				433					
			173	1600	G. -22.6	441	85.3		
		213	2450	G. -18.2	305	81.7			
[40]	404.14	3193	403	R.G. -34.3	216	—	Both: RO3010 (10.2, 0.0035)	1.235	
			433	R.G. -30.6	213	—			
			868	R.G. -26.6	211	—			
			915	R.G. -26.0	205	—			
			2450	R.G. -18.4	203	—			
This work	114.70	750	403	G. -41.5	555	87.5	Cufion (2.05, 0.00045)/No	0.456	
			433	G. -39.5	563	86.6			
			611	G. -32.9	636	88.2			
			868	G. -30.5	624	90.5			
			928	G. -30.0	579	84.0			
		160	1395	G. -27.6	599	81.3			
			1432	G. -27.3	575	84.6			

## VI. CONCLUSION

In this work, a novel miniaturized multi-track muscle implantable planar patch antenna has been proposed for WIMDs biomedical telemetry communications. The patch slotting and a pair of open-end slots in the ground plane techniques have been used to obtain a wideband and multi-band behavior. The miniaturized antenna compact volume of  $114.70 \text{ mm}^3$  was implemented with a low relative permittivity substrate and does not require any superstrate. Seven telemetry allocated frequency bands are covered widely starting from the lower frequency band of MedRadio (401–406) MHz to the WMTS (1.427–1.432) GHz. A prototype of the proposed antenna has been fabricated, and the agreement between simulation and measurement was fully in free space.

Antenna's operation was investigated in two realistic implantations of human body, in the underneath the scalp and in the upper part of the arm.

Considering the three performance criteria, 1) optimized volume of the antenna, 2) total number of seven largely covered allocated frequency bands, and 3) peak gain values at considered frequencies at once, the proposed implantable antenna is very satisfactory compared to many recent proposed implantable antennas referenced in this work.

A model for the link communication distance is adopted and ascertained by performing computations for the cases of free space and indoor propagation environments.

With seven telemetry bands covered, the proposed implanted antenna is a candidate for various clinical applications of the head and arm. It can also be designed with a full ground plane and still cover five telemetry frequency bands. In addition, a second mode of antenna implantation, i.e., in the skin, can also be used with five operating frequency bands covered.

## ACKNOWLEDGMENT

We would like to thank Mr. Erwan Fichou for his assistance in the manufacture of the antennas and the IUT of Chartres for his financial support.

## REFERENCES

- [1] P. S. Hall and Y. Hao, *Antennas and Propagation for Body Centric Wireless Communications*, Artech House, Norwood, 2012.
- [2] K. S. Nikita, *Handbook of Biomedical Telemetry*, Wiley-IEEE, 2014.
- [3] A. Kiourti and K. S. Nikita, "A review of in-body biotelemetry devices: Implantables, ingestibles, and injectables," *IEEE Transactions on Biomedical Engineering*, vol. 64, no. 7, pp. 1422-1430, Jul. 2017. doi: 10.1109/TBME.2017.2668612.
- [4] A. K. Teshome, B. Kibret, and D. T. H. Lai, "A review of implant communication technology in WBAN: Progress and challenges," *IEEE Reviews in Biomedical Engineering*, vol. 12, pp. 88-99, Feb. 2019. doi: 10.1109/RBME.2018.2848228.
- [5] K. Fujimoto and K. Ito, *Antennas for Small Mobile Terminals*, Artech House, Norwood, 2018.
- [6] Z. N. Chen, D. Liu, H. Nakano, X. Qing, and Th. Zwick, *Handbook of Antenna Technologies*, Springer, Singapore, 2016.
- [7] S. Bakogianni and S. Koulouridis, "An implantable planar dipole antenna for wireless MedRadio-Band biotelemetry devices," *IEEE Antennas and Wireless Propagation Letters*, vol. 15, pp. 234-237, Feb. 2016. doi: 10.1109/LAWP.2015.2439039.
- [8] S. M. Huang, M. R. Tofighi, and A. Rosen, "Consideration for the design and placement of implantable annular slot antenna for intracranial pressure monitoring devices," *IEEE Antennas and Wireless Propagation Letters*, vol. 14, pp. 1514-1517, Jul. 2015. doi: 10.1109/LAWP.2014.2370940.
- [9] C. Wang, L. Zhang, S. Wu, S. Huang, C. Liu, and X. Wu, "A dual-band monopole antenna with EBG for wearable wireless body area networks," *Applied Computational Electromagnetics Society (ACES) Journal*, vol. 36, no. 1, pp. 48-54, Jan. 2021. <https://doi.org/10.47037/2020.ACES.J.360107>.
- [10] D. Nikolayev, M. Zhadobov, and R. Sauleau, "Impact of tissue electromagnetic properties on radiation performance of in-body antennas," *IEEE Antennas and Wireless Propagation Letters*, vol. 17, no. 8, pp. 1440-1444, Aug. 2018. doi: 10.1109/LAWP.2018.2848943.
- [11] X. Y. Liu, Z. T. Wu, Y. Fan, and E. M. Tentzeris, "A miniaturized CSRR loaded wide-beamwidth circularly polarized implantable antenna for subcutaneous real-time glucose monitoring," *IEEE Antennas and Wireless Propagation Letters*, vol. 16, pp. 577-580, Mar. 2017. doi: 10.1109/LAWP.2016.2590477.
- [12] A. Kiourti, J. R. Costa, C. A. Fernandes, and K. S. Nikita, "A broadband implantable and a dual-band on-body repeater antenna: Design and transmission performance," *IEEE Transactions on Antennas and Propagation*, vol. 62, no. 6, pp. 2899-2908, Jun. 2014. doi: 10.1109/TAP.2014.2310749.
- [13] C. Tsai, K. Chen, and C. Yang, "Implantable wideband low-SAR antenna with c-shaped coupled ground," *IEEE Antennas and Wireless Propagation Letters*, vol. 14, pp. 1594-1597, Aug. 2015. doi: 10.1109/LAWP.2015.2413839.
- [14] H. Li, Y. Guo, and S. Xiao, "Broadband circularly polarised implantable antenna For biomedical

- applications,” *Electronics Letters*, vol. 52, no. 7, pp. 504-506, Apr. 2016. doi: 10.1049/el.2015.4445.
- [15] A. G. Miquel, S. Curto, N. Vidal, J. M. Lopez-Villegas, F. M. Ramos, and P. Prakash, “Multilayered broadband antenna for compact embedded implantable medical devices: Design and characterization,” *Progress In Electromagnetics Research*, vol. 159, pp. 1-13, Apr. 2017. doi:10.2528/PIER16121507
- [16] Y. Zhang, C. Liu, X. Liu, K. Zhang, and X. Yang, “A wideband circularly polarized implantable antenna for 915 MHz ISM-Band biotelemetry devices,” *IEEE Antennas and Wireless Propagation Letters*, vol. 17, no. 8, pp. 1473-1477, Aug. 2018. doi: 10.1109/LAWP.2018.2849847.
- [17] S. Das and D. Mitra, “A compact wideband flexible implantable slot antenna design with enhanced gain,” *IEEE Transactions on Antennas and Propagation*, vol. 66, no. 8, pp. 4309-4314, Aug. 2018. doi: 10.1109/TAP.2018.2836463.
- [18] R. Lesnik, N. Verhovski, I. Mizrachi, B. Milgrom, and M. Haridim, “Gain enhancement of a compact implantable dipole for biomedical applications,” *IEEE Antennas and Wireless Propagation Letters*, vol. 17, no. 10, pp. 1778-1782, Oct. 2018. doi: 10.1109/LAWP.2018.2866233.
- [19] G. Samanta and D. Mitra, “Miniaturised and radiation efficient implantable antenna using reactive impedance surface for biotelemetry,” *IET Microwaves, Antennas & Propagation*, vol. 14, no. 2, pp. 177-184, Feb. 2020. doi: 10.1049/iet-map.2019.0132.
- [20] X. Yang, H. Wong, and J. Xiang, “Polarization reconfigurable planar inverted-F antenna for implantable telemetry applications,” *IEEE Access*, vol. 7, pp. 141900-141909, Oct. 2019. doi: 10.1109/ACCESS.2019.2941388.
- [21] Z. Xia, H. Li, Z. Lee, S. Xiao, W. Shao, X. Ding, and X. Yang, “A wideband circularly polarized implantable patch antenna for ISM band biomedical applications,” *IEEE Transactions on Antennas and Propagation*, vol. 68, no. 3, pp. 2399-2404, Mar. 2020. doi: 10.1109/TAP.2019.2944538.
- [22] A. Kiourt and K. S. Nikita, “Miniature scalp-implantable antennas for telemetry in the MICS and ISM bands: Design, safety considerations and link budget analysis,” *IEEE Transactions on Antennas and Propagation*, vol. 60, no. 8, pp. 3568-3575, Aug. 2012. doi: 10.1109/TAP.2012.2201078.
- [23] J. Ung and T. Karacolak, “A dual-band meandered Dipole antenna for medical telemetry applications,” *Progress In Electromagnetics Research C*, vol. 63, pp. 85-94, Apr. 2016. doi:10.2528/PIERC16012603
- [24] S. A. A. Shah and H. Yoo, “Scalp-implantable antenna systems for intracranial pressure monitoring,” *IEEE Transactions on Antennas and Propagation*, vol. 66, no. 4, pp. 2170-2173, Apr. 2018. doi: 10.1109/TAP.2018.2801346.
- [25] A. O. Kaka, M. Toycan, S. D. Walker, and D. Kavaz, “Dual band, miniaturized, implantable antenna design with on-body antennas for wireless health monitoring,” *Applied Computational Electromagnetics Society (ACES) Journal*, vol. 35, no. 4, pp. 443-452, Apr. 2020.
- [26] L. Xu, Y. Guo, and W. Wu, “Dual-band implantable antenna with open-end slots on ground,” *IEEE Antennas and Wireless Propagation Letters*, vol. 11, pp. 1564-1567, 2012. doi: 10.1109/LAWP.2012.2237010.
- [27] M. Usluer, B. Cetindere, and S. C. Basaran, “Compact implantable antenna design for MICS and ISM band biotelemetry applications,” *Microwave and Optical Technology Letters*, vol. 62, no. 4, pp. 1581-1587, Apr. 2020. <https://doi.org/10.1002/mop.32185>.
- [28] Y. Fan, H. Liu, X. Liu, Y. Cao, Z. Li, and M. M. Tentzeris, “Novel coated differentially fed dual-band fractal antenna for implantable medical devices,” *IET Microwaves, Antennas & Propagation*, vol. 14, no. 2, pp. 199-208, Feb. 2020. doi: 10.1049/iet-map.2018.6171.
- [29] F. Faisal and H. Yoo, “A miniaturized novel-shape dual-band antenna for implantable applications,” *IEEE Transactions on Antennas and Propagation*, vol. 67, no. 2, pp. 774-783, Feb. 2019. doi: 10.1109/TAP.2018.2880046.
- [30] H. Zhang, L. Li, C. Liu, Y.-X. Guo, and S. Wu, “Miniaturized implantable antenna integrated with split ring resonate rings for wireless power transfer and data telemetry,” *Microwave and Optical Technology Letters*, vol. 59, no. 3, pp. 710-714, Mar. 2017. <https://doi.org/10.1002/mop.30381>
- [31] L. Luo, B. Hu, J. Wu, T. Yan, and L.-J. Xu, “Compact dual-band antenna with slotted ground for implantable applications,” *Microwave and Optical Technology Letters*, vol. 61, no. 5, pp. 1314-1319, May 2019. <https://doi.org/10.1002/mop.31718>.
- [32] I. Gani and H. Yoo, “Multi-band antenna system for skin implant,” *IEEE Microwave and Wireless Components Letters*, vol. 26, no. 4, pp. 294-296, Apr. 2016. doi: 10.1109/LMWC.2016.2538470.
- [33] R. Das, Y. Cho, and H. Yoo, “High efficiency unidirectional wireless power transfer by a triple band deep-tissue implantable antenna,” *2016 IEEE MTT-S International Microwave Symposium (IMS)*, San Francisco, CA, pp. 1-4, 2016. doi: 10.1109/MWSYM.2016.7540252.

- [34] M. Zada and H. Yoo, "A miniaturized triple-band implantable antenna system for bio-telemetry applications," *IEEE Transactions on Antennas and Propagation*, vol. 66, no. 12, pp. 7378-7382, Dec. 2018. doi: 10.1109/TAP.2018.2874681.
- [35] F. Huang, C. Lee, C. Chang, L. Chen, T. Yo, and C. Luo, "Rectenna application of miniaturized implantable antenna design for triple-band biotelemetry communication," *IEEE Transactions on Antennas and Propagation*, vol. 59, no. 7, pp. 2646-2653, Jul. 2011. doi: 10.1109/TAP.2011.2152317.
- [36] C. K. Wu, T. F. Chien, C. L. Yang, and C. H. Luo, "Design of novel s-shaped quad-band antenna for MedRadio/WMTS/ISM implantable biotelemetry applications," *Int. J. Antennas Propag.*, vol. 2012, Article ID 564092, 2012. doi:10.1155/2012/564092.
- [37] I. A. Shah, M. Zada, and H. Yoo, "Design and analysis of a compact-sized multiband spiral-shaped implantable antenna for scalp implantable and leadless pacemaker systems," *IEEE Transactions on Antennas and Propagation*, vol. 67, no. 6, pp. 4230-4234, Jun. 2019. doi: 10.1109/TAP.2019.2908252.
- [38] A. Basir and H. Yoo, "Efficient wireless power transfer system with a miniaturized quad-band implantable antenna for deep-body multitasking implants," *IEEE Transactions on Microwave Theory and Techniques*, vol. 68, no. 5, pp. 1943-1953, May 2020. doi: 10.1109/TMTT.2020.2965938.
- [39] A. Kiourti and K. S. Nikita, "A review of implantable patch antennas for biomedical telemetry: challenges and solutions [wireless corner]," *IEEE Antennas and Propagation Magazine*, vol. 54, no. 3, pp. 210-228, Jun. 2012. doi: 10.1109/MAP.2012.6293992.
- [40] Z. Jiang, Z. Wang, M. Leach, E. G. Lim, J. Wang, R. Pei, and Y. Huang, "Wideband loop antenna with split-ring resonators for wireless medical telemetry," *IEEE Antennas and Wireless Propagation Letters*, vol. 18, no. 7, pp. 1415-1419, Jul. 2019. doi: 10.1109/LAWP.2019.2918501.
- [41] Available on 08.04.2021. <https://www.craneae.com/microwave-solutions-substrates>
- [42] S. Gabriel, R. W. Lau, and C. Gabriel, "The dielectric properties of biological tissues," *Phys. Med. Biol.*, vol. 41, pp. 2231-2293, 1996. Available at: <http://niremf.ifac.cnr.it/tissprop/>
- [43] C. M. Lee, T. C. Yo, F. J. Huang, and C. H. Luo, "Bandwidth enhancement of planar inverted-f antenna for implantable biotelemetry," *Microwave and Optical Technology Letters*, vol. 51, no. 3, pp. 749-752, Mar. 2009. <https://doi.org/10.1002/mop.2418>
- [44] S. N. Makarov, G. M. Noetscher, J. Yanamadala, M. W. Piazza, S. Louie, A. Proko, A. Nazarian, and A. Nummenmaa, "Virtual human models for electromagnetic studies and their applications," *IEEE Reviews in Biomedical Engineering*, vol. 10, pp. 95-121, Dec. 2017. doi: 10.1109/RBME.2017.2722420.
- [45] IEEE Standard for Safety Levels with Respect to Human Exposure to Radiofrequency Electromagnetic Fields, 3 kHz to 300 GHz, IEEE Standard C95.1, 1999.
- [46] IEEE Standard for Safety Levels with Respect to Human Exposure to Radiofrequency Electromagnetic Fields, 3 kHz to 300 GHz, IEEE Standard C95.1, 2005.
- [47] International Telecommunications Union-Radiocommunications (ITU-R), Radio Regulations, document SA 1346, ITU, Geneva, Switzerland. Available at: <http://itu.int/home>



**Mohamed Behih** was born in Bordj Bou Arreridj, Algeria, in 1981. He received the Engineer degree in electronic engineering and the Magister degree in communication from Setif University, Algeria, in 2004 and 2007, respectively. He is currently working toward the Doctor of Sciences degree in communication.

From 2010 to 2015, he was an Assistant Professor with the Electronics Department, University of Blida, Algeria. He is presently working as an Assistant Professor with Bordj Bou Arreridj University, Algeria. His researches focus on biomedical engineering, interaction between electromagnetic wave and human body, medical devices and biomedical telemetry, and antennas for wireless body area networks.



**Farid Bouttout** received the B.Sc. and M.Sc. degrees in electronic engineering from the University of Constantine, Constantine, Algeria, in 1994 and 1997, respectively, and the Ph.D. degree in electronic engineering from the University of Setif, Setif, Algeria, in 2001. He was granted three-year postdoc study on design of planar antennas for medical applications at the Commissariat à l'Énergie Atomique (CEA) and at the University of Paris VI, France.

He is currently a Professor with the Electronics Department, University of Bordj Bou Arreridj. His current research interests include planar and cylin-

dical microstrip antennas and transmission lines, computational electromagnetics, high performance computing, neural networks, and fuzzy logic.



**Tarek Fortaki** was born on March 31, 1972, in Constantine, Algeria. He received the Engineer of Communication degree in 1995, the Master of Science degree in microwaves in 1999, and the Doctorate degree in microwaves in 2004, all from the Electronics

Department, Faculty of Engineering Science, University of Constantine.

Currently, he is a Professor with the Electronics Department, Faculty of Technology, University of Batna 2. He has published more than 40 papers in refereed journals and more than 50 papers in conference proceedings. He serves as a Reviewer for several technical journals. His main research interests are in electromagnetic

theory, numerical methods, and modeling of antennas and passive microwave circuits.



**Christophe Dumond** was born in Tulle, France, on October 22, 1966. He received the Ph.D. degree in optic communications and microwaves from the University of Limoges, France, in 1994. His works concern the electromagnetic answer of wire structures to fast trans-

sient perturbations.

In 2007, he joined the Institut Pluridisciplinaire de Recherche en Ingénierie des Systèmes Mécaniques et Energétique (PRISME), University of Orléans, France. His fields of research include fractal antennas, high Tc superconducting microstrip patch, phased arrays, and implantable antennas for bio-telemetry. He is also a teacher and head of the Electrical Engineering Department, Institut Universitaire de Technologie (IUT), Chartres, France.